Crashworthiness design and optimisation of windowed tubes under axial impact loading

Hamid Nikkhah[1], Ahmad Baroutaji[2*], Abdul Ghani Olabi[3, 4]

(1) Faculty of Engineering, School of Mechanical Engineering, University of Mohaghegh Ardabili, Ardabil, Iran

(2) School of Engineering, Faculty of Science and Engineering, University of Wolverhampton, Telford, UK

(3) Dept. of Sustainable and Renewable Energy Engineering, University of Sharjah, P.O. Box 27272, Sharjah, UAE

(4) School of Engineering and Applied Science, Aston University, Aston Triangle, Birmingham B4 7ET, UK

Abstract

Thin-walled structures are frequently used as energy absorbers in the automotive, railway and aviation industries. This paper addresses the crashworthiness performance of thin-walled windowed tubes under dynamic impact loading. Different shapes of cut-outs were introduced to thin-walled tubes with different cross-sectional shapes to create windowed tubes. Explicit finite element code, LS-DYNA, was used to simulate the crushing behaviour of the windowed tubes under axial impact loading. The Finite Element (FE) model was validated by conducting experimental tests and showing that the numerical and experimental responses are comparable. The crashworthiness responses of the different windowed tubes were compared and the best performing tube was identified using a multi-criteria decision-making method known as Technique of Order Preference by Similarity to Ideal Solution (TOPSIS). It was found that a circular tube with a square window shape outperforms all other sections and exhibits the best energy absorption characteristics.

Subsequently, a multi-objective optimisation analysis was performed to find the optimal configuration of the best tube. Response Surface Methodology (RSM) was used to develop

models for the energy absorption responses of the tube. The design variables were selected to describe size, number, and distributions of the windows, while specific energy absorption (SEA) and peak crush force (PCF) were set as design responses. Parametric analysis was conducted to understand the effects of the design variables on the crashworthiness behaviour and the optimal configuration was identified.

Keywords

Windowed tube, Energy absorption Impact, Dynamic loading, crashworthiness, optimisation

1. Introduction

Thin-walled structures are widely used in aerospace and automotive industries as energy absorption components that protect occupants during a collision event [1]. During an impact event, thin-walled tubes crush progressively dissipating the impact energy and thus reducing the influence of impact forces on the passengers. The goal for an engineer is to design a system that provides the maximum protection for the occupants against impact generated from vehicle accidents. This means that the thin-walled structures must increase the energy absorption and decrease the impact force for the safety of passengers. Thus, the design requirements for improving the crashworthiness performance of thin-walled structures are high SEA, low PCF and high Crush Force Efficiency (CFE).

The energy absorption behaviour of thin-walled structures was studied under different types of loading including axial loading [2], [3], lateral loading [4]–[10], oblique loading [11], and bending loading [12], [13].

For example, Tran and Baroutaji [11] investigated the crashworthiness behaviour of multi-cell triangular tubes under axial and oblique loading. They have employed a multi-objective optimization algorithm to find the optimal design of the tube under multiple loading cases. Fang

et al [14] used multi-objective robust design optimisation method to find the optimal crashworthiness design of foam-filled bitubal structures. Baroutaji and co-authors [5], [8] studied the crush and energy absorption behaviour of circular and oblong tubes under lateral loading and obtained the optimal design for each one of them.

Among the various types of deformation modes, the axial crushing mode was identified as the most effective mode for energy absorption as most of the tube's material deforms plastically thus making use of the majority of the tube's mass [1]. With an aim of improving the energy absorption behaviour of thin-walled structures, tubes with unconventional shapes or materials have been adopted such as multi-cell tubes [15], [16], functionally graded thickness tubes [17], [18], foam-filling tubes [14], [19]–[22], corrugated tubes [23], grooved tubes [24], [25], and windowed tubes [26]–[28]. Eyvazian et al [23] investigated experimentally and theoretically the axial crushing behaviour of tubes with shallow and deep corrugations. Their results showed that corrugated tubes demonstrate excellent energy absorption characteristics in terms of more uniform force-displacement curve, lower of initial peak load, and controllable failure mechanism.

Embedding cut-outs or windows on the walls of thin-walled tubes were introduced as a mean of reducing the initial peak force and improving the overall crashworthiness behaviour of the tubes [28]–[33]. Gupta et al [34], [35] studied the crush response of circular tubes which contain circular holes on their walls. They found that the holes reduced the initial impact force and helped in avoiding the overall buckling when the slenderness ratio (length to diameter) was large. A confirmation of the advantages of the windowed tubes was presented by Song et al [36]–[38] who studied the crashworthiness behaviour of thin-walled square tubes with patterned windows. The authors found that by introducing windows on the tube wall, the energy absorption

characteristics such as initial peak force and energy absorption capacity could be significantly improved. Also, H. Nikkhah et al [26] investigated the effect of the hole's shape on the crashworthiness of square tubes under dynamic loading condition. Their research showed that rectangular and square-shaped holes provide the best crashworthiness performance for the square tubes.

Despite the excellent crashworthiness performance of the windowed tubes, they only received limited interest from researchers. No attempt was made in the literature to compare the crashworthiness behaviour of windowed tubes with different cross-sectional shape for both the tubes and the windows. Thus, in this study, the crush behaviour and energy absorption capability of a new set of windowed tubes are investigated, compared, and optimised.

2. Material and Methods

2.1 Geometrical description of windowed tubes

Tubes with three different cross-sectional shapes including circular, hexagonal and square as shown in Figure 1, were tested in this study. All these tubes have the same cross-section area of 1225 mm^2, a length of 90 mm, and a wall thickness of 2 mm. Three shapes of holes namely circular, hexagonal and square were introduced to the previous tubes to create windowed tubes. The holes, i.e. windows, have the same cross section area of 78.5 mm^2 and distributed equally along the length of the tubes as shown in Figure 2. The distance between the top (bottom) of the tube is 10 mm and the distance between holes is 23.35mm.

2.2 Finite Element Modelling

Explicit Finite Element (FE) software package, LS-DYNA, was adopted for simulating the axial crushing of the windowed tubes. The FE model is consisted of three main parts including, the upper moving base, the thin-walled tube, and the lower stationary base, as shown in Figure 3.

The upper base is modelled as a rigid body and constrained to travel along the axial direction of the tube. The bottom base was also modelled as a rigid body where its movement was constrained in all directions so it became stationary. The bottom end of the tube is fixed onto the bottom base while the top of the tube is free. The rigid upper base, with a mass of 500 kg and moves at a velocity of 15 m/sec, impacts the tube at its top end. The mass was chosen to ensure full deformation of the tube while the impact speed is a typical value used for the automobile crashworthiness applications [39]. A Belytschko-Tsay 4-node shell element with 5 integration points through the thickness is used to mesh the model because it is suitable for the large deformation of thin-walled tubes [26]. A mesh sensitivity analysis was performed to determine the optimal mesh size of the finite element model as shown in Figure 4. An element size of 1 mm, which results in a total number of elements of 50000, was found to provide a good convergence for both crashworthiness responses within reasonable solution time and thus it was used throughout this study. Automatic single surface and surface to surface contacts with a friction coefficient of 0.15 were used to represent the tubes self-contact and tube-to-wall contact, respectively. The tubes were made of aluminium alloy AA6060-T4 with a density of 2700kg/m^3, Young's modulus of 68 GPa, and Poisson's ratio of 0.33. Tensile tests were performed using a universal test machine to obtain the true stress-strain curve of the material, as shown in Figure 5. The Mat_Piecewise_Linear_Plasticity model #24 in LS-DYNA was used to represent the material behaviour of the aluminium alloy AA6060 T4 during the crushing process. Since aluminium alloy is insensitive to strain rate under dynamic load, the material strain rate effects were ignored in this study [40].

2.3 Multi-objective optimisation

Formulation of optimisation problem

A multi-objective optimisation problem is given by a general mathematical formulation as shown in equation 1:

$$\begin{cases} \text{Minimise} & f(x) = [f_1(x), f_2(x), \ldots., f_i(x)] \\ s.t & x^l \leq x \leq x^u \end{cases} \quad 1$$

Where $x=(x_1,x_2,\ldots, x_k)$ is the vector of k design variables, x_l and x_u are respectively the lower and upper bounds of the design variables, f(x) are the objective functions. Among the various crashworthiness characteristics, SEA and PCF, as shown in Figure 6, were selected as design responses in this study.

A thin-walled energy absorber should absorb the maximum possible amount of energy per unit mass, in order to allow for a lightweight design with efficient fuel consumption and thus the SEA should be maximised. Also, in order to avoid the severe injury and reduce the jerking effects felt by the occupants in the survival space, the crushing of the energy absorber should not lead to high decelerations and this can be achieved by minimising PCF. Factors describing the size, number, and distributions of windows including the characteristic dimension of the holes (d), the number of holes in the horizontal direction (N_h), and the number of holes in the vertical direction (N_v) were selected as design variables.

Response Surface Methodology (RSM) and optimisation algorithm

RSM is a set of mathematical and statistical techniques that can be used for modelling the responses of a specific engineering system as functions of the controllable input variables. Generally, the Response Surface (RS) model can be expressed by equation 2

$$Y = f\ (x_1, x_2, \ldots\ldots, x_k) \quad 2$$

Where: k is the number of independent variables

If a second order polynomial function is used in RSM to describe the relationship between the responses and the independent variables then the RS model is given as in equation 3

$$y = b_o + \sum b_i x_i + \sum b_{ij} x_i x_j + \sum b_{ii} x_{ii}^2 + \varepsilon \qquad 3$$

Where $b_o, b_i\ ,\ b_{ij}, b_{ii}$ known as regression coefficients of the model, ε is unobserved random error.

In the current study, RSM was used to construct models which relate the crashworthiness responses, i.e. SEA and PCF, to different design variables. The advantage of employing RSM is that the crashworthiness responses in a particular design space can be identified through performing a reduced number of experiments or simulations at sampling design points. The sampling design points can be generated using different methods offered by Design of Experiment (DoE) such as factorial, Box–Behnken design (BBD), central-composite design (CCD) and D-optimal. The adequacy of the developed Response Surface (RS) models is checked via the analysis of variance (ANOVA) to confirm their capability in predicting the crashworthiness responses accurately. Various statistical measures, R-square parameter, Adjusted R-square, and Adeq Precision, were used to confirm the statistical significance of the models. Once the RS models have been developed and tested for adequacy, they can be used in the multi-objective optimisation formula. Desirability approach was used to solve the multi-objective crashworthiness optimisation problem as denoted in equation 1. This technique has received considerable attention for solving the multi-objective crashworthiness optimisation problems due to its simplicity, low computational cost and rapid convergence [5], [7], [8], [41]. In this approach, all multiple crashworthiness responses, i.e. SEA and PCF, are combined into a single non-dimensional objective function, called an overall desirability function, which only

generates one solution for the optimisation problem. The main steps for using the desirability approach in the multi-objective optimisation problem are detailed in Figure 7.

2.4 TOPSIS method

TOPSIS method is used in this study to identify the tube with best crashworthiness performance in terms of both SEA and PCF responses. TOPSIS, an abbreviation of Technique of Order Preference by Similarity to Ideal Solution, is a multiple criteria decision-making method which allows determining the best candidate among others based on multiple responses [42], [43]. It has received increased attention for crashworthiness investigations [26], [44]. In this method, it is assumed that among the different candidates there is positive ideal candidate and negative ideal candidate where the former has the best level for all attributes considered and the latter has the worst level. A candidate gets higher score if it is closer to the positive ideal candidate and further from the negative ideal candidate [43].

TOPSIS can be implemented in the current design problem as follows;

Firstly a design matrix (X), which is consisted of m candidates and n criteria, should be constructed. This design matrix maps the candidates, i.e. different windowed tubes, to the selection criteria, i.e. crashworthiness responses including SEA and PCF. Each element of this matrix (x_{ij}) is the value of candidate i with respect to criterion j.

Secondly, the design matrix is normalised as shown in equation 4

$$r_{ij} = \frac{x_{ij}}{\sqrt{\sum_{k=1}^{m} x_{kj}^2}} \qquad 4$$

In which r_{ij} is the element of normalised design matrix R.

Thirdly, each criterion is assigned a weight factor. In the present study, all criteria have the same weight and thus this step has no effect on the final score of each tube.

Fourthly, from the matrix R, both positive ideal and negative ideal candidates can be determined. Positive ideal candidate (A^+) has lowest PCF and highest SEA while negative ideal candidate (A^-) has highest PCF and lowest SEA among all candidates. The distance of the ith candidate to the ideal positive and negative candidates, denoted by D_i^+ or D_i^-, is given by equation 5

$$D_i^{+/-} = \sqrt{\sum_{j=1}^{n} (r_{ij} - A_j^{+/-})^2} \qquad 5$$

The relative closeness of each candidate to the ideal candidates is calculated by the following equation 6

$$S_i^+ = \frac{D_i^-}{D_i^+ + D_i^-} \qquad 6$$

In which S_i^+ is the relative closeness of the i_{th} candidate. The candidate with S^+ closer to 1 is the best candidate.

3. Results and discussion

3.1 Experimental validation of FE model

To validate the FE model, axial crushing tests were conducted on different configurations of simple and windowed tubes. The geometrical configurations of the tubes used in the experiments along with the experimental set-up are shown in Figure 8. The tests were performed using a universal test machine (type STM-150) where a sample was placed between the bottom stationary and the top moving bases. The crushing process was quasi-static with a crushing speed of 10 mm/min. Figure 9 shows the crushing response and deformation modes obtained from experiments and simulations. It can be seen that the finite element models of the different tubes provide excellent predictions for force-displacement curves as well as the deformation modes of

the tubes. As a result, the FE model in this paper can be considered as an accurate model and can be extended to model the other simple and windowed tubes.

3.2 Crush analysis of windowed tubes with different geometrical shape

In this section, the crushing performance of simple and windowed tubes with different geometrical shapes is investigated. SEA and PCF responses were used to evaluate and compare the crashworthiness behaviour of the different tubes. The force-displacement curves, SEA and PCF responses, and deformation modes of all tubes are shown in Figure 10Figure 12, respectively. Generally, the windowed tubes allow for using longer tubes without undergoing the global bending mode [34]. However, for the current study, both simple and windowed tubes have the same length and they are all deformed progressively where none of them undergoes the inefficient global bending mode. Furthermore, it can be seen from the deformation modes, Figure 12, that the simple tubes have a more desirable symmetrical deformation mode with shorter wavelengths and greater number of folds than those observed in the windowed tubes. This is due to the fact that the simple tubes have a uniform material distribution at the deformation locations and this makes the axial stiffness of these tubes more uniform than the windowed tubes, which have material discontinuities, leading to a more regular deformation pattern. The deformation modes of circular windowed tubes, as shown in Figure 12, are irregular and their crush response, as depicted in Figure 10 (a), are quite different from each other. This indicates that the collapse behaviour of such structures is sensitive to the window profile. On the other hand, the crushing behaviour of square and hexagonal windowed tubes was less sensitive to the change in the window profile where the force-displacement responses of these structures, as shown in Figure 10 (b and c), exhibit slight difference when changing the geometrical shape of the windows. Also, both simple and windowed tubes exhibit similar trend for force-displacement response in

which the crushing forces increase sharply to initial peak values and then start fluctuating periodically around a mean value in a fashion corresponding to the formation of folds during the crushing. However, the windowed tubes offer lower PCF and also lower fluctuation in the post-collapse stages. With regards to SEA and PCF responses, simple tubes show higher SEA and PCF for all cross-section shapes. This is due to the fact that the plastic deformation in the windowed tubes is initiated at the windows region which has less material and thus it requires less force to initiate the collapse and absorbs lower energy compared to the simple tubes.

3.3 Identifying the best windowed tube using TOPSIS

TOPSIS method, which is a multi-criteria decision-making method, was used with SEA and PCF responses to determine the best performing windowed tube. In the present study, there are 12 candidates, as shown in Figure 2, and each one has two crashworthiness metrics, i.e. SEA and PCF, so the total number of criteria is 24, as shown in Table 1. The final score and ranking of each tube obtained by the application of TOPSIS method are presented in Table 2. It can be seen that circular tube with square window (C-S) is the best in the overall performance while the simple square tube (S) has the lowest ranking.

3.4 Parametric analysis and optimisation of the best windowed tube

Response Surface (RS) models of SEA and PCF

Central-composite design (CCD) was adopted to create the sampling design points in this study. CCD is highly efficient sampling strategy that allows for creating accurate RS models with lower number of experiments. The geometrical parameters of the created windows including the width of the window (d), the number of windows in the horizontal direction (N_h), and the number of windows in the vertical direction (N_v) were selected as design variables. The upper and lower limits of the geometrical parameters for all sampling points are illustrated in Table 3. FE models were created for the C-S windowed tubes with the geometrical parameters corresponding to the

sampling design points, as shown in Figure 13, and the crashworthiness responses were determined. The different combinations of the design variables with corresponding design responses are tabulated in Table *4*. The RS models of the SEA and PCF in terms of the geometrical factors of the holes are shown in equations 7 and 8, respectively

$$(SEA)^3 = 14984.6 - 1061.62 \times d + 514.3 \times N_h + 627.7 \times N_v - 263.33 \times N_h \times N_v \quad 7$$

$$(PCF)^{0.01} = 1.035 + 1.14 \times 10^{-4} \times d + 5.97 \times 10^{-4} \times N_h - 1.13 \times 10^{-4} \times N_v - 1.78 \times 10^{-4} \times d \times N_h \quad 8$$

The accuracy of the aforementioned RS models was checked using Analysis of Variance (ANOVA) statistical technique. Table 5 summarises the statistical measurements for the developed RS models for SEA and PCF. As it can be seen that all models show high F-value and very low P-value which confirm that these models are significant. Additionally, both models exhibit high enough values of adequate precision ratios which are greater than 4 and this means that the models have insignificant noise. Additionally, the RS models show high values of R-squared (coefficient of determination) and they also exhibit a very good agreement between the predicted and adjusted R-squared values. The relationship between the actual responses, obtained from the simulations, and those predicted by the developed RS models are shown in Figure 14. It is clear that the residuals are close to the diagonal line which also confirms that the predictive capabilities of the developed RS models are very good. All of the aforementioned measurements prove that the developed RS models are accurate and valid and thus they can be used to navigate the whole design space.

Parametric analysis of the C-S windowed tube

The crashworthiness responses of windowed C-S tube depend strongly on the windows parameters including the size, number and distribution. Thus, parametric analysis of these responses was conducted using the developed RS models in the previous section.

3.4.2.1 Effect of design variables on SEA

Figure 15 demonstrates the changes of SEA with d and N_v for two different values of N_h. It can be seen that the SEA tends to increase with decreasing all design variables, i.e. d, N_v, and N_h. The energy absorption capacity under axial loading is dominated by the amount of material available to be plastically deformed [1]. Introducing the windows on the side walls of the tube reduces the amount of the material at the deformation regions and this reduces the energy absorption capacity. The larger the windows are, the less the material that can undergo plastic deformation is. Thus, decreasing the number and size of windows means that there is more material in the tube to be deformed plastically and participate in the energy absorption process. By inspecting the figure closely, it can be seen that the influence of N_v on SEA response is almost insignificant when the N_h is small and it becomes more obvious by increasing the number of windows in the horizontal direction. This is generally due to the effect of interaction between N_h and N_v on the SEA which makes the rate of change of SEA with N_v depends strongly on the setting of N_h. Among all design variables, the window size, d, is the most dominant variable to influence of the SEA response. For a tube with maximum number of holes in both horizontal and vertical directions, increasing d from 4 mm to 8 mm causes a decrease of 19% in the SEA. It is clear that a tube with d of 8 mm, N_v of 5, and N_h of 6 absorb the lowest amount of energy per unit mass.

3.4.2.2 Effect of design variables on PCF

Figure 16 illustrates the variation of PCF with d and N_v for N_h of 2 and 6, respectively. It is evident from these plots that PCF decreases when the size and number of windows increases. Generally, a C-S tube with smaller size and less number of windows contains more material and thus it requires a greater magnitude of force to initiate the crushing process. Obviously, a C-S tube with d of 4 mm, N_v of 1, and N_h of 2 has the highest PCF. Despite the C-S tubes with higher number and/or bigger size of windows may absorb lower SEA, they would generate lower PCF during their crushing and this can be seen as an advantage for the safety of the occupants. A C-S tube with smaller size and lower number of windows produces a PCF which is 37% less than its counterpart with the highest number and size of windows. Meanwhile, the SEA drops only by 26% when using a tube with more windows. Concerning the PCF response, the window size seems to be the most influencing factor while N_h and N_v are the second and least influencing factors, respectively. This can be explained by the fact that the plastic deformation begins with formation one fold at either location of the windows so the bigger the windows are, the less the material is left at the region and hence a lower PCF is needed to initiate the crushing. Since PCF only corresponds to a formation of the first fold during the deformation process, the influence of the number of windows on PCF is insignificant. For example, when N_v and N_h set at maximum values, increasing the window size from 4 mm to 8 mm decreases the magnitude of PCF from 30.28 kN to 20.92 kN; which account for a 31% decrease in PCF. Similarly, for maximum values of d and N_h, varying the N_v from maximum to minimum values only change PCF by 4.4%.

3.4.2.3 Effect of design variables on deformation modes

Figure 17 exhibits the deformation mode of C-S tubes representing the design points. It is clear that all C-S tubes have maintained a progressive collapse mode and none of them has undergone the inefficient global bending one. The sample C-S-7 which has a moderate number of windows with small size seems to have the best crushing mode with shorter wavelength and greater number of folds. This trend might be due to the fact that the small size windows are more efficient in redistributing the axial load which in turn makes the stiffness of the tube more uniform leading to a more regular deformation mode. Samples with bigger window size such as (C-S=1, C-S-3, C-S-6, and C-S-13) tend to develop lower number of folds during the crushing. This is because the windows with bigger size promote the creation of folds with greater wavelength and this, in turn, reduces the number of folds generated during the total deformation process. Additionally, it is evident from the deformation modes reported in Figure 17 that the tubes with bigger windows have irregular deformation modes and this is consistent with the findings of other studies [36]. Another observation that can be reported from Figure 17 is that the moderate number of windows in the vertical direction seems to promote a better deformation mode with higher number of folds as it can be seen in C-S-4, C-S-5, C-S-7, and C-S-12.

Multi-objective optimisation results

The final multi-objective crashworthiness optimisation formula of the windowed tubes in terms of SEA and PCF as design responses, and d, N_h, and N_v as design variables can be expressed as in equation 9:

$$\begin{cases} Maxmise & \mathrm{SEA} = f_1(\mathrm{d}, N_h, N_v) \\ Minmise & \mathrm{PCF} = f_2(\mathrm{d}, N_h, N_v) \\ s.t & 4 \le \mathrm{d} \le 8 \\ s.t & 2 \le N_h \le 6 \\ s.t & 1 \le N_v \le 5 \end{cases} \quad (9)$$

The desirability approach was used to solve the above equation. Figure 18 shows a contour plot of the desirability objective as a function of d and N_v at upper and lower limits of N_h. It is clear that desirability increases as d and N_h increases while N_v decreases. The greatest desirability was obtained in a tube with d of 8 mm, N_h of 6, and N_v of 1. Thus, the one can conclude that the optimal shape of the windowed tube can be obtained by increasing d, increasing the number of holes in the horizontal direction and decreasing the number of holes in the vertical direction.

To validate the optimisation results, the crashworthiness responses of the optimal tube were obtained by constructing a FE model. The force-displacement response of the optimal tube, as well as a comparison between the numerical results and RS results, are shown in Figure 19. It is clear that the numerical results are in excellent agreement with those obtained from the optimisation algorithm which inferno the validity of the optimised results.

4. Conclusion

In this paper, cut-outs with different shapes were introduced to thin-walled structures with different cross-sectional profiles including circular, square, and hexagonal to create windowed tubes. The crushing and energy absorption behaviour of these tubes were studied under axial dynamic loading via experimental tests and numerical simulations. The numerical models were created using LS-DYNA and validated with experimental tests. The crashworthiness responses of the different simple and windowed tubes were computed. The results revealed that the windowed tubes exhibit less PCF than the simple tubes and this was considered as an advantage for the windowed tubes over their simple counterparts. However, the simple tubes showed higher SEA and better deformation mode than the windowed tubes. The performance of the different tubes was compared and ranked using TOPSIS with PCF and SEA as design criteria. The circular tube with square windows has the highest score and was selected as the best tube in the

study with better combined SEA and PCF responses. Finally, RSM and desirability approach were used to analyse and optimise the best performing tube. It was found that the optimal tube is the one that has bigger window size, higher number of windows in the horizontal directions but lower number of holes in the vertical direction.

5. References

[1] A. Baroutaji, M. Sajjia, and A.-G. Olabi, "On the crashworthiness performance of thin-walled energy absorbers: Recent advances and future developments," *Thin-Walled Struct.*, vol. 118, pp. 137–163, Sep. 2017.

[2] Z. Fan, G. Lu, and K. Liu, "Quasi-static axial compression of thin-walled tubes with different cross-sectional shapes," *Eng. Struct.*, vol. 55, pp. 80–89, Oct. 2013.

[3] X. Zhang and H. Huh, "Crushing analysis of polygonal columns and angle elements," *Int. J. Impact Eng.*, vol. 37, no. 4, pp. 441–451, Apr. 2010.

[4] A. Baroutaji and A.-G. A. G. Olabi, "Analysis of the Effect of the Elliptical Ratio in Tubular Energy Absorbers Under Quasi-Static Conditions," in *Advanced Structured Materials*, vol. 16, A. Öchsner, L. F. M. da Silva, and H. Altenbach, Eds. Berlin, Heidelberg: Springer Berlin Heidelberg, 2012, pp. 323–336.

[5] A. Baroutaji, M. D. Gilchrist, D. Smyth, and A. G. Olabi, "Crush analysis and multi-objective optimization design for circular tube under quasi-static lateral loading," *Thin-Walled Struct.*, vol. 86, pp. 121–131, 2015.

[6] A. Baroutaji, M. D. Gilchrist, and A. G. Olabi, "Quasi-static, impact and energy absorption of internally nested tubes subjected to lateral loading," *Thin-Walled Struct.*,

vol. 98, pp. 337–350, Jan. 2016.

[7] A. Baroutaji, M. D. Gilchrist, D. Smyth, and A. G. Olabi, “Analysis and optimization of sandwich tubes energy absorbers under lateral loading,” *Int. J. Impact Eng.*, vol. 82, pp. 74–88, Aug. 2015.

[8] A. Baroutaji, E. Morris, and A. G. Olabi, “Quasi-static response and multi-objective crashworthiness optimization of oblong tube under lateral loading,” *Thin-Walled Struct.*, vol. 82, pp. 262–277, Sep. 2014.

[9] A. Niknejad, S. M. Elahi, S. A. Elahi, and S. A. Elahi, “Theoretical and experimental study on the flattening deformation of the rectangular brazen and aluminum columns,” *Arch. Civ. Mech. Eng.*, vol. 13, no. 4, pp. 449–464, 2013.

[10] A. Baroutaji and A. G. Olabi, “Lateral collapse of short-length sandwich tubes compressed by different indenters and exposed to external constraints,” *Materwiss. Werksttech.*, vol. 45, no. 5, p. n/a-n/a, May 2014.

[11] T. Tran and A. Baroutaji, “Crashworthiness optimal design of multi-cell triangular tubes under axial and oblique impact loading,” *Eng. Fail. Anal.*, vol. 93, pp. 241–256, Nov. 2018.

[12] X. Zhang, H. Zhang, and Z. Wang, “Bending collapse of square tubes with variable thickness,” *Int. J. Mech. Sci.*, vol. 106, pp. 107–116, Feb. 2016.

[13] I. Duarte, M. Vesenjak, L. Krstulovic-Opara, and L. Krstulovi??-Opara, “Dynamic and quasi-static bending behaviour of thin-walled aluminium tubes filled with aluminium foam,” *Compos. Struct.*, vol. 109, no. 1, pp. 48–56, 2014.

[14] J. Fang, Y. Gao, G. Sun, Y. Zhang, and Q. Li, “Crashworthiness design of foam-filled bitubal structures with uncertainty,” *Int. J. Non. Linear. Mech.*, vol. 67, pp. 120–132, Dec. 2014.

[15] T. Tran, S. Hou, X. Han, W. Tan, and N. Nguyen, “Theoretical prediction and crashworthiness optimization of multi-cell triangular tubes,” *Thin-Walled Struct.*, vol. 82, pp. 183–195, Sep. 2014.

[16] S. Hou, Q. Li, S. Long, X. Yang, and W. Li, “Multiobjective optimization of multi-cell sections for the crashworthiness design,” *Int. J. Impact Eng.*, vol. 35, no. 11, pp. 1355–1367, Nov. 2008.

[17] G. Sun, F. Xu, G. Li, and Q. Li, “Crashing analysis and multiobjective optimization for thin-walled structures with functionally graded thickness,” *Int. J. Impact Eng.*, vol. 64, pp. 62–74, Feb. 2014.

[18] J. Fang, Y. Gao, G. Sun, G. Zheng, and Q. Li, “Dynamic crashing behavior of new extrudable multi-cell tubes with a functionally graded thickness,” *Int. J. Mech. Sci.*, vol. 103, pp. 63–73, Nov. 2015.

[19] Z. Ahmad, D. P. P. Thambiratnam, and A. C. C. C. C. Tan, “Dynamic energy absorption characteristics of foam-filled conical tubes under oblique impact loading,” *Int. J. Impact Eng.*, vol. 37, no. 5, pp. 475–488, May 2010.

[20] Z. Ahmad and D. P. Thambiratnam, “Dynamic computer simulation and energy absorption of foam-filled conical tubes under axial impact loading,” *Comput. Struct.*, vol. 87, no. 3–4, pp. 186–197, Feb. 2009.

[21] A. Niknejad, B. Rezaei, and G. H. Liaghat, “Empty circular metal tubes in the splitting process - Theoretical and experimental studies,” *Thin-Walled Struct.*, vol. 72, pp. 48–60, 2013.

[22] A. Niknejad and D. M. Rahmani, “Experimental and theoretical study of the lateral compression process on the empty and foam-filled hexagonal columns,” *Mater. Des.*, vol. 53, pp. 250–261, Jan. 2014.

[23] A. Eyvazian, T. N. Tran, and A. M. Hamouda, “Experimental and theoretical studies on axially crushed corrugated metal tubes,” *Int. J. Non. Linear. Mech.*, vol. 101, pp. 86–94, May 2018.

[24] C. W. Isaac and O. Oluwole, “Structural response and performance of hexagonal thin-walled grooved tubes under dynamic impact loading conditions,” *Eng. Struct.*, vol. 167, pp. 459–470, Jul. 2018.

[25] P. Xu, C. Yang, Y. Peng, S. Yao, J. Xing, and B. Li, “Cut-out grooves optimization to improve crashworthiness of a gradual energy-absorbing structure for subway vehicles,” *Mater. Des.*, 2016.

[26] H. Nikkhah, F. Guo, Y. Chew, J. Bai, J. Song, and P. Wang, “The effect of different shapes of holes on the crushing characteristics of aluminum square windowed tubes under dynamic axial loading,” *Thin-Walled Struct.*, vol. 119, no. June, pp. 412–420, 2017.

[27] A. Taştan, E. Acar, M. A. Güler, and Ü. Kılınçkaya, “Optimum crashworthiness design of tapered thin-walled tubes with lateral circular cutouts,” *Thin-Walled Struct.*, vol. 107, pp. 543–553, 2016.

[28] A. G. Mamalis, D. E. Manolakos, K. N. Spentzas, M. B. Ioannidis, S. Koutroubakis, and P. K. Kostazos, “The effect of the implementation of circular holes as crush initiators to the crushing characteristics of mild steel square tubes: experimental and numerical simulation,” *Int. J. Crashworthiness*, vol. 14, no. 5, pp. 489–501, Sep. 2009.

[29] S. Lee, C. Hahn, M. Rhee, and J.-E. Oh, “Effect of triggering on the energy absorption capacity of axially compressed aluminum tubes,” *Mater. Des.*, vol. 20, no. 1, pp. 31–40, Mar. 1999.

[30] C. Zhou, S. Ming, C. Xia, B. Wang, X. Bi, P. Hao, and M. Ren, “The energy absorption of rectangular and slotted windowed tubes under axial crushing,” *Int. J. Mech. Sci.*, vol. 141, pp. 89–100, Jun. 2018.

[31] H. Han, F. Taheri, and N. Pegg, “Quasi-static and dynamic crushing behaviors of aluminum and steel tubes with a cutout,” *Thin-Walled Struct.*, vol. 45, no. 3, pp. 283–300, Mar. 2007.

[32] S. Pirmohammad and S. Esmaeili-Marzdashti, “Multi-objective crashworthiness optimization of square and octagonal bitubal structures including different hole shapes,” *Thin-Walled Struct.*, vol. 139, pp. 126–138, Jun. 2019.

[33] A. G. Mamalis, D. E. Manolakos, K. N. Spentzas, M. B. Ioannidis, S. Koutroubakis, and P. K. Kostazos, “The effect of the implementation of circular holes as crush initiators to the crushing characteristics of mild steel square tubes: experimental and numerical simulation,” *Int. J. Crashworthiness*, vol. 14, no. 5, pp. 489–501, Sep. 2009.

[34] N. K. Gupta and S. K. Gupta, “Effect of annealing, size and cut-outs on axial collapse

behaviour of circular tubes," *Int. J. Mech. Sci.*, vol. 35, no. 7, pp. 597–613, Jul. 1993.

[35] N. K. Gupta, "Some aspects of axial collapse of cylindrical thin-walled tubes," *Thin-Walled Struct.*, vol. 32, no. 1–3, pp. 111–126, Sep. 1998.

[36] J. Song, Y. Chen, and G. Lu, "Light-weight thin-walled structures with patterned windows under axial crushing," *Int. J. Mech. Sci.*, vol. 66, pp. 239–248, Jan. 2013.

[37] J. Song, "Numerical simulation on windowed tubes subjected to oblique impact loading and a new method for the design of obliquely loaded tubes," *Int. J. Impact Eng.*, vol. 54, pp. 192–205, Apr. 2013.

[38] J. Song and F. Guo, "A comparative study on the windowed and multi-cell square tubes under axial and oblique loading," *Thin-Walled Struct.*, vol. 66, pp. 9–14, May 2013.

[39] G. M. Nagel and D. P. Thambiratnam, "Dynamic simulation and energy absorption of tapered thin-walled tubes under oblique impact loading," *Int. J. Impact Eng.*, vol. 32, no. 10, pp. 1595–1620, Oct. 2006.

[40] L. Aktay, B.-H. Kröplin, A. K. Toksoy, and M. Güden, "Finite element and coupled finite element/smooth particle hydrodynamics modeling of the quasi-static crushing of empty and foam-filled single, bitubular and constraint hexagonal- and square-packed aluminum tubes," *Mater. Des.*, vol. 29, no. 5, pp. 952–962, Jan. 2008.

[41] A. Baroutaji, "Energy absorption through the lateral collapse of thin-walled single and nested tubes," *Baroutaji, Ahmad Energy Absorpt. through lateral collapse thin-walled single nested tubes. PhD thesis, Dublin City Univ.*, 2014.

[42] C. L. (Ching-L. Hwang and K. Yoon, *Multiple Attribute Decision Making : Methods and Applications A State-of-the-Art Survey*. Springer Berlin Heidelberg, 1981.

[43] C.-L. Hwang, Y.-J. Lai, and T.-Y. Liu, "A new approach for multiple objective decision making," *Comput. Oper. Res.*, vol. 20, no. 8, pp. 889–899, Oct. 1993.

[44] S. Pirmohammad and S. Esmaeili Marzdashti, "Crashworthiness optimization of combined straight-tapered tubes using genetic algorithm and neural networks," *Thin-Walled Struct.*, vol. 127, pp. 318–332, Jun. 2018.

Table 1: Initial peak force (PCF) and SEA of each tube

Circular Tube			*Hexagonal Tube*			*Square Tube*		
Tube	PCF (kN)	SEA (kJ/kg)	Tube	PCF (kN)	SEA (kJ/kg)	Tube	PCF(kN)	SEA (kJ/kg)
C	37.4	23.0	H	35.3	21.5	S	38.4	19.0
C-C	26.8	18.2	H-C	29.5	19.9	S-C	32.8	17.9
C-H	26.4	18.4	H-H	29.2	19.6	S-H	32.5	17.8
C-S	27.1	20.4	H-S	29.7	20.4	S-S	33.3	19.3

Table 2: Score and rank of all tubes obtained by TOPSIS method

Tube	Score	Rank
C	0.0733	7
C-C	0.1018	6
C-H	0.1051	3
C-S	0.1248	1
H	0.0711	8
H-C	0.1050	4
H-H	0.1034	5
H-S	0.1089	2
S	0.0203	12
S-C	0.0594	11
S-H	0.0614	10
S-S	0.0648	9

Table 3: Upper and lower bounds of the design variables

Design variable	Lower limit	Upper limit
d	4 mm	8 mm
N_h	2	6
N_v	1	5

Table 4: Design matrix					
Tube	d (mm)	N_h	N_v	SEA (kJ/kg)	PCF (kN)
C-S-1	8	2	5	19.8618	28.4067
C-S-2	4	2	1	23.186	31.5129
C-S-3	8	6	1	20.355	22.285
C-S-4	6	6	3	20.8589	24.4002
C-S-5	6	4	3	21.109	27.9502
C-S-6	8	6	5	16.2499	20.7521
C-S-7	4	4	3	21.9073	32.6355
C-S-8	4	2	5	23.1407	31.4422
C-S-9	4	6	5	21.0532	29.8993
C-S-10	4	6	1	23.1846	31.7561
C-S-11	6	4	1	22.2282	30.0647
C-S-12	8	4	3	20.6164	24.9148
C-S-13	8	2	1	18.7664	29.5044
C-S-14	6	4	5	20.4815	28.6518
C-S-15	6	2	3	21.4	32.1318

Table 5: Summary of ANOVA analysis for the developed RS of SEA and PCF responses

Model	F-Value	P-Value	Statistical measurements			
			R^2	Adj-R^2	Pre-R^2	Adeq Precision
$SEA = f(d, N_h, N_v)$	27.52	<0.0001	0.91	0.88	0.81	18.26
$PCF = f(d, N_h, N_v)$	52.4	<0.0001	0.95	0.93	0.9	22.5

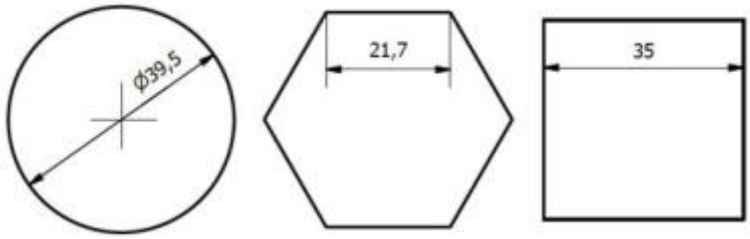

Figure 1: Different cross-section

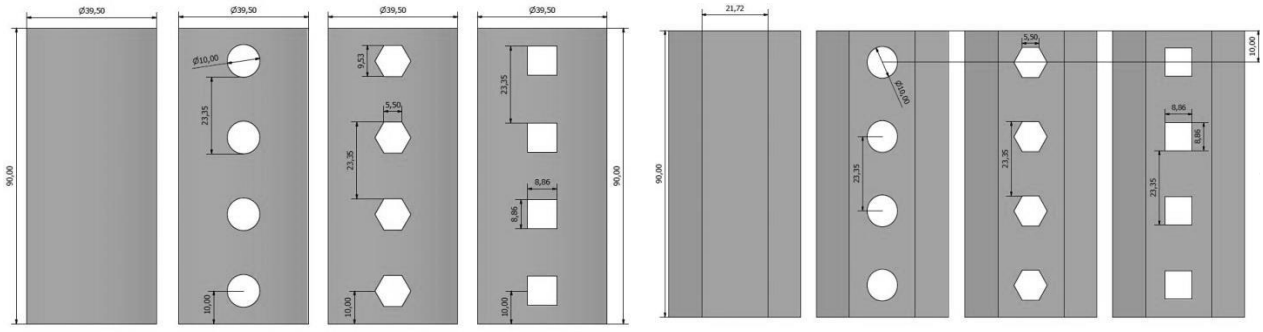

a) Left to right (C, C-C, C-H, C-S) b) Left to right (H, H-C, H-H, H-S)

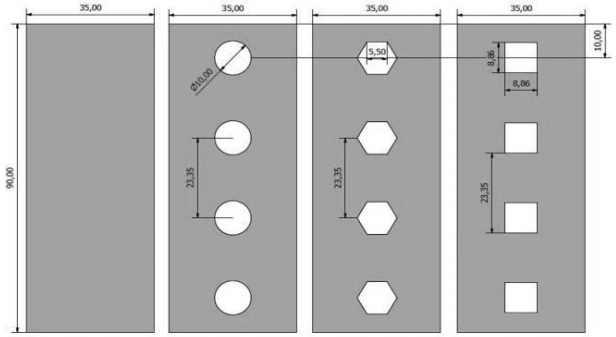

c) Left to right (S, S-C, S-H, S-S)

Figure 2: Windowed tubes: a) Circular, b) Hexagonal, c) Square

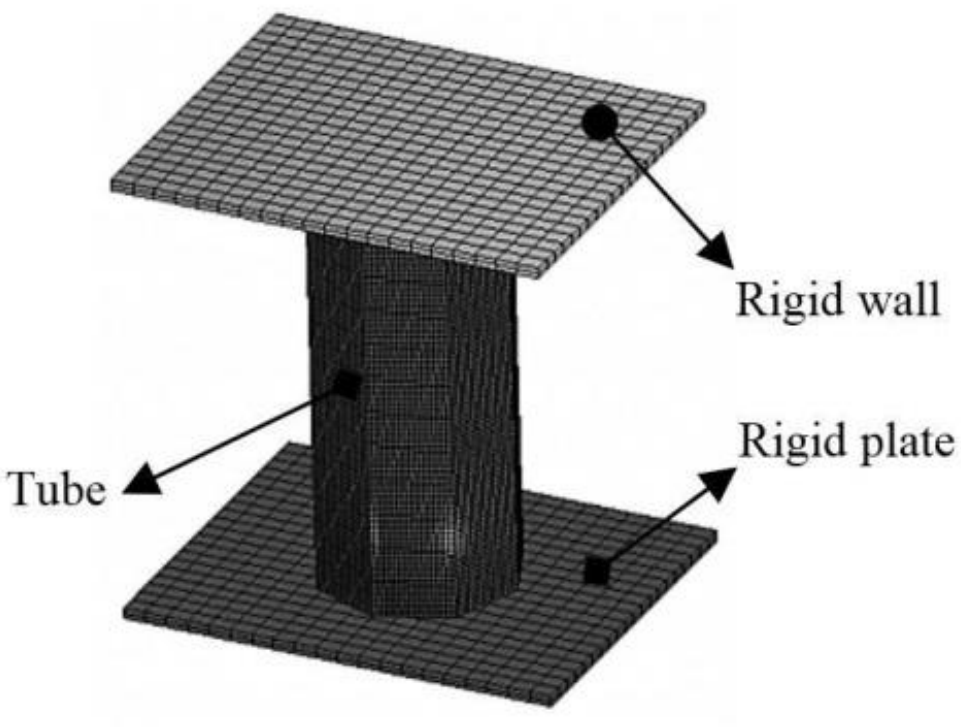

Figure 3: Schematic of finite element model of H tube under axial loading

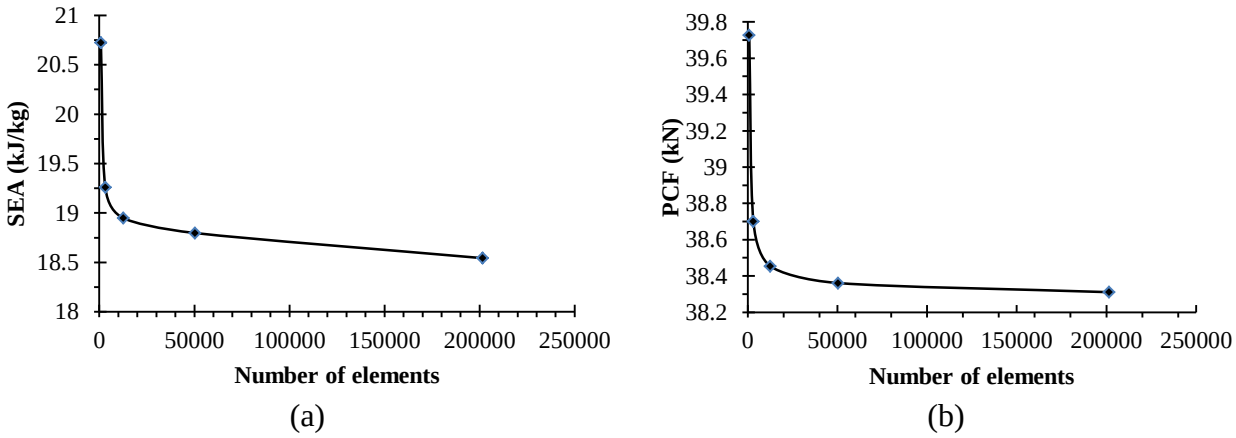

Figure 4: Mesh convergence of (a) SEA response, and (b) PCF response for a simple square tube

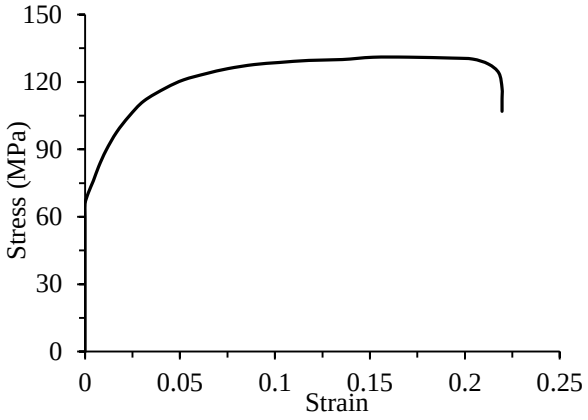

(a)

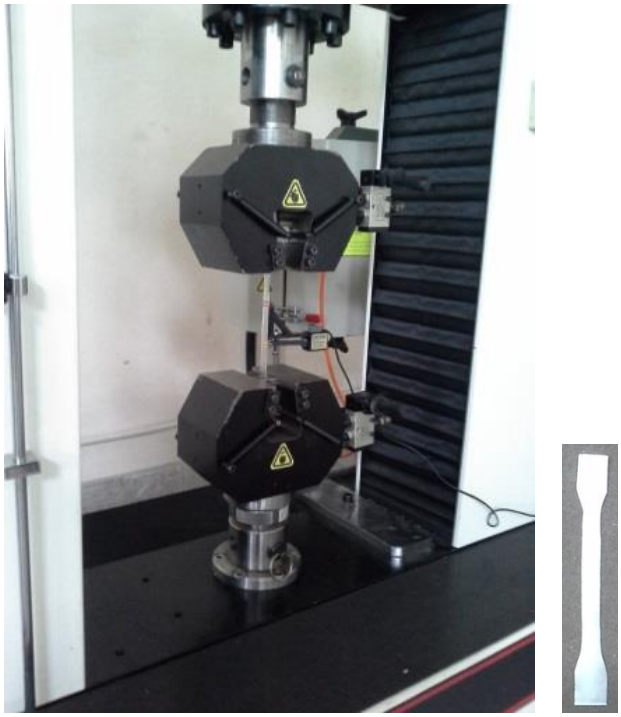

(b)

Figure 5: Tensile test: a) True stress-strain of AL6060-T4, b) Universal test machine (STM-150)

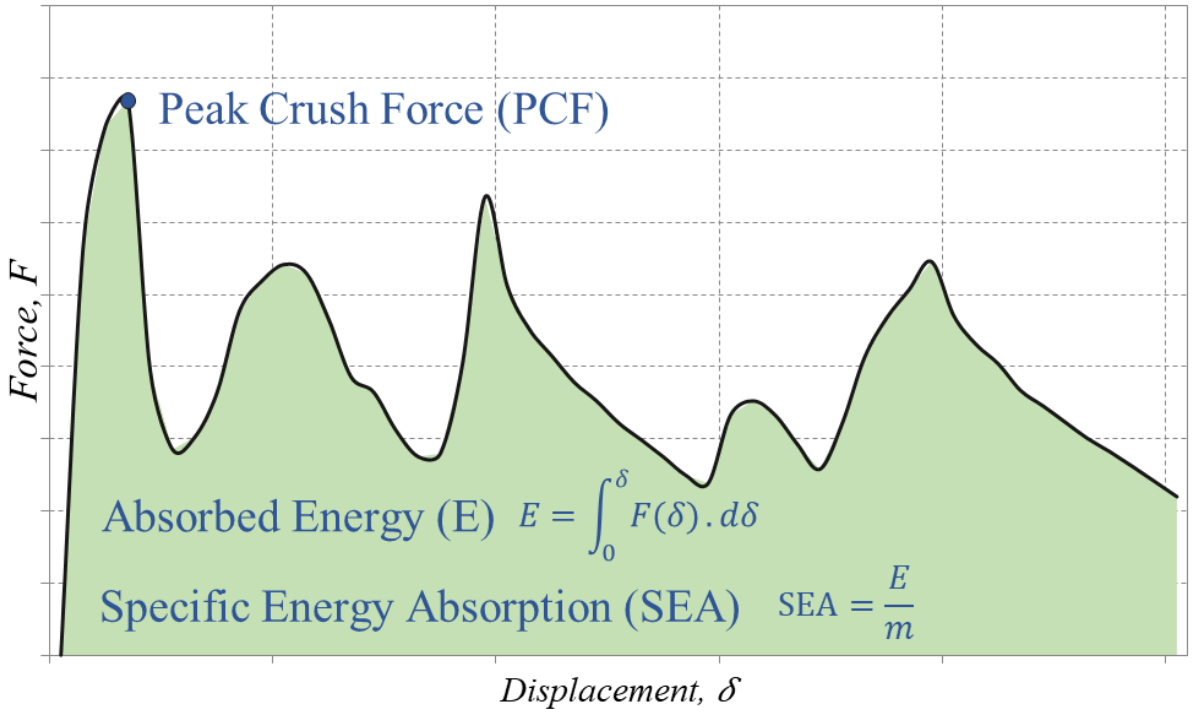

Figure 6: Typical crush force-displacement response under axial loading with explanation of SEA and PCF responses

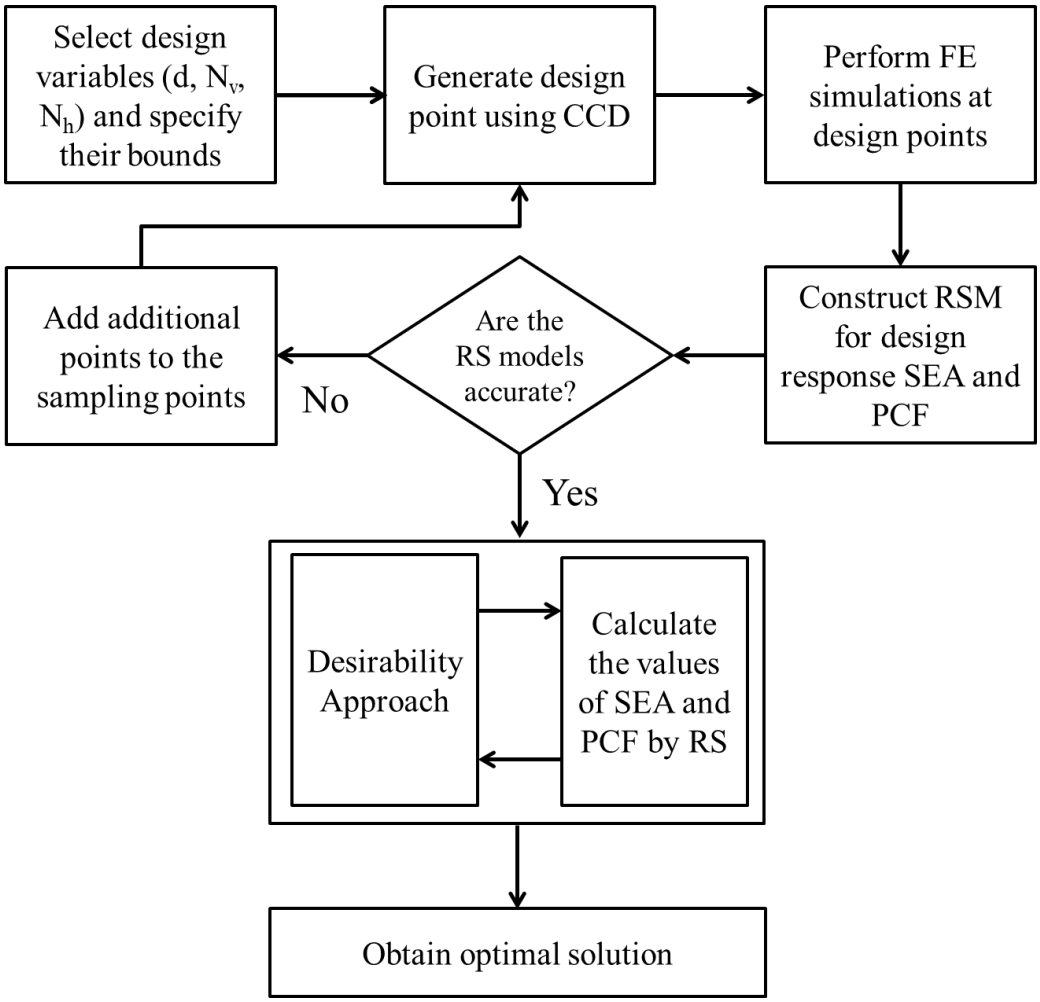

Figure 7: Flow chart of optimisation scheme using the desirability approach

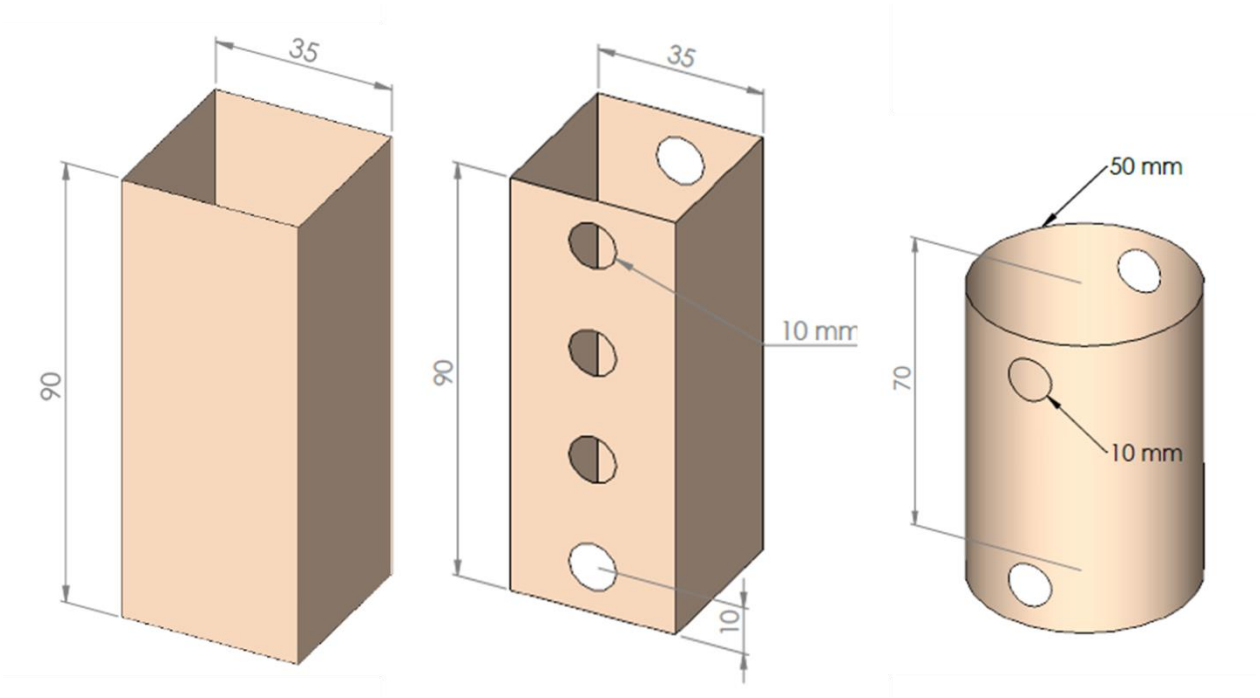

(a)

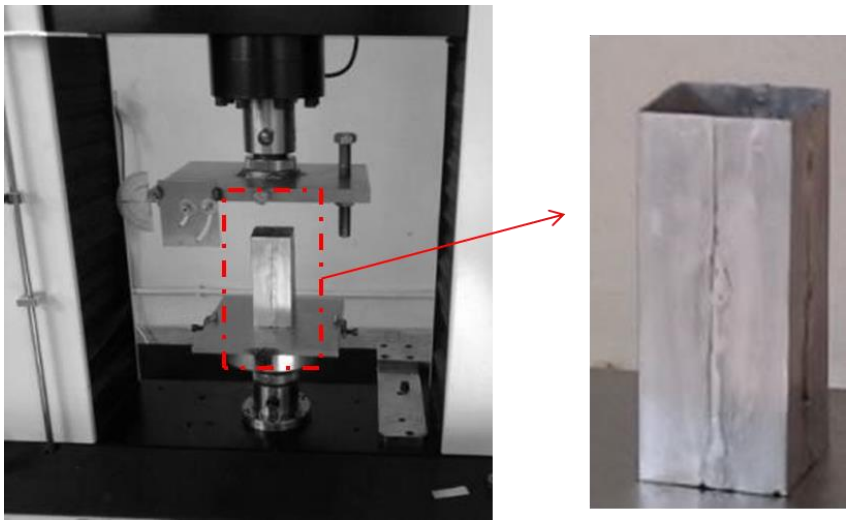

(b)

Figure 8: (a) Geometrical details of samples used for FEM validation (b) Experimental test setup

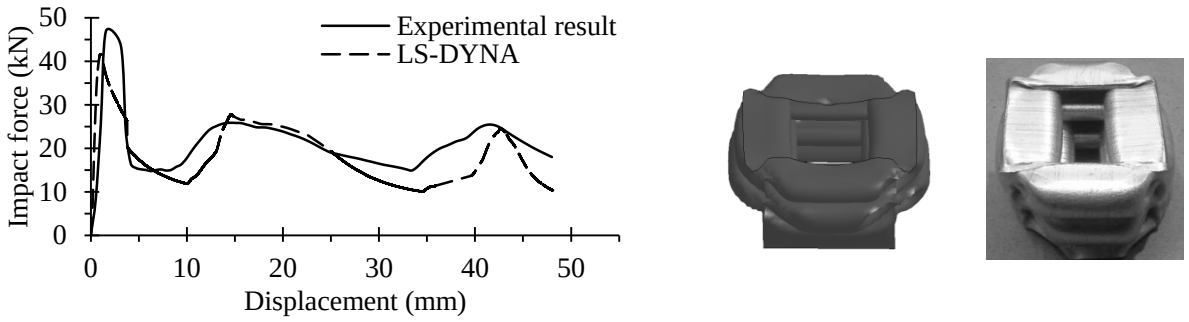

(a)

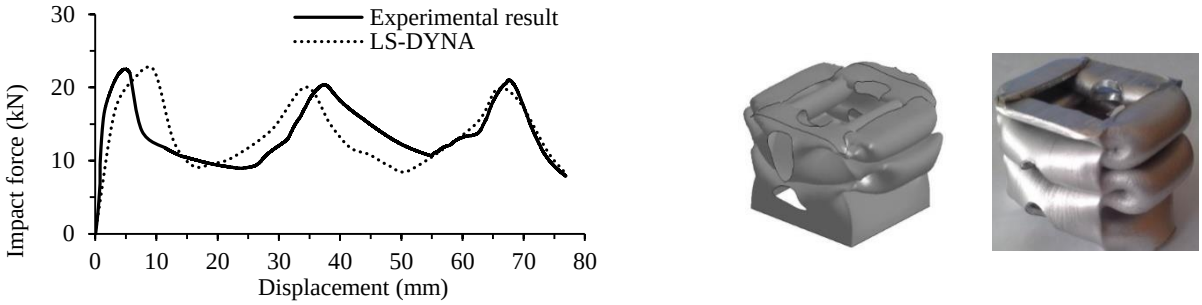

(b)

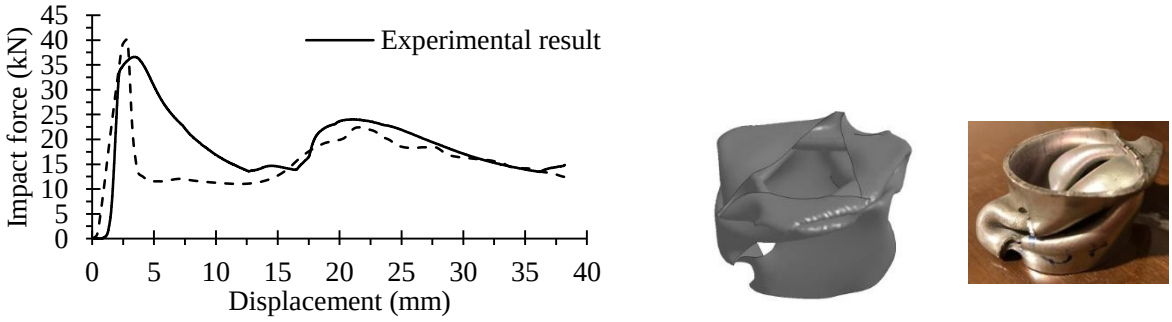

(c)

Figure 9: Comparison of experimental and simulation results: (a) Simple square tube (b) Windowed square tube (c) Windowed circular tube

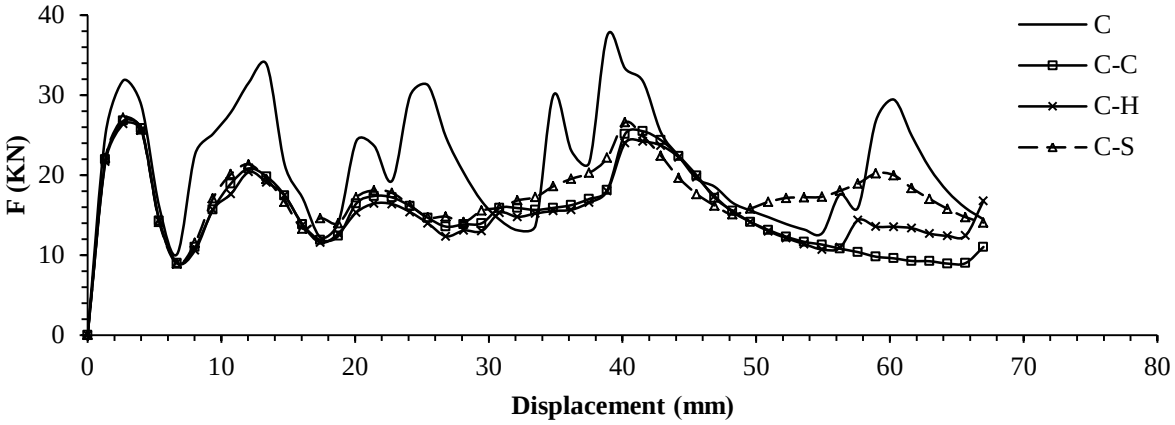

(a)

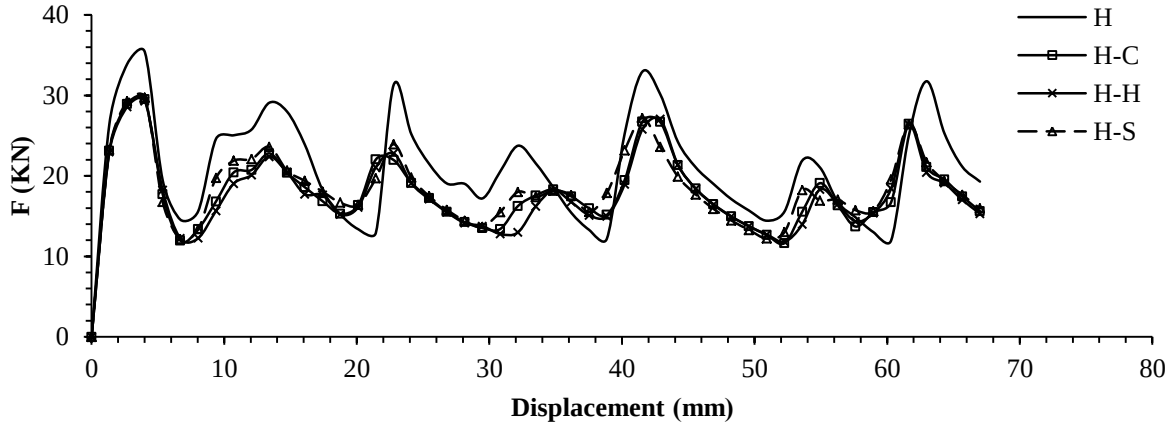

(b)

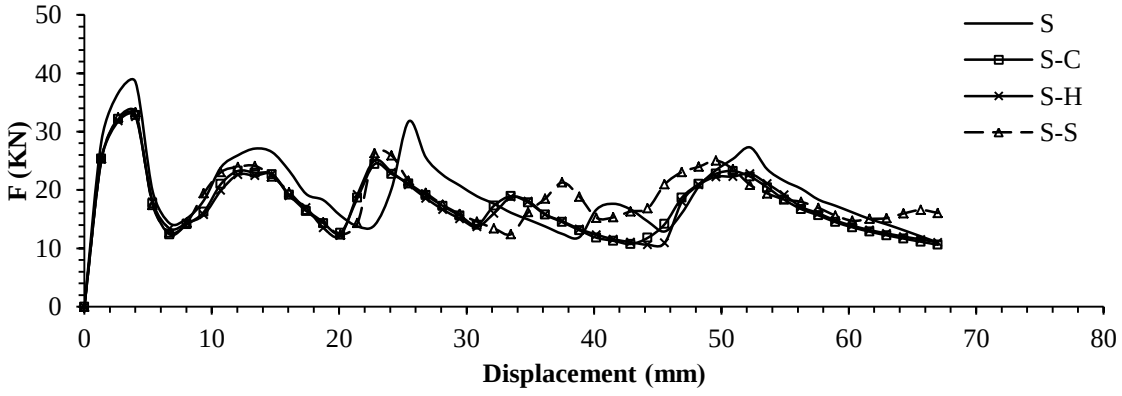

(c)

Figure 10: Force-displacement curves: a) Circular tube, b) Hexagonal tube, c) Square tube

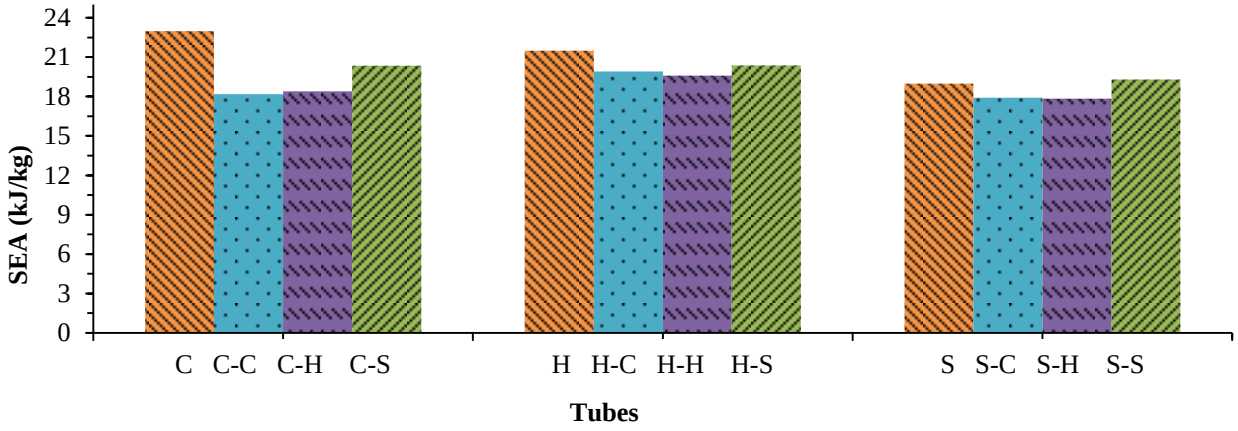

(a)

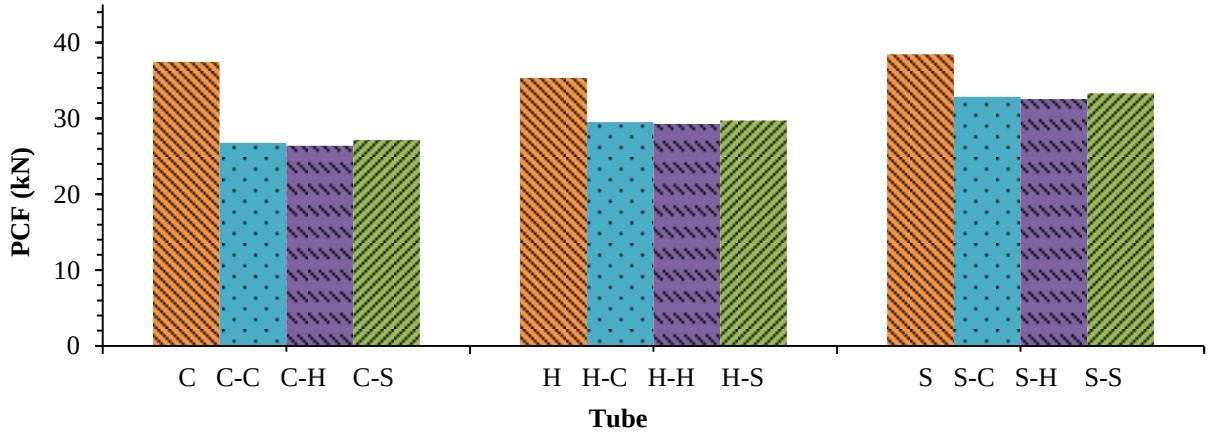

Figure 11: Crashworthiness responses for all tube a) SEA, b) PCF

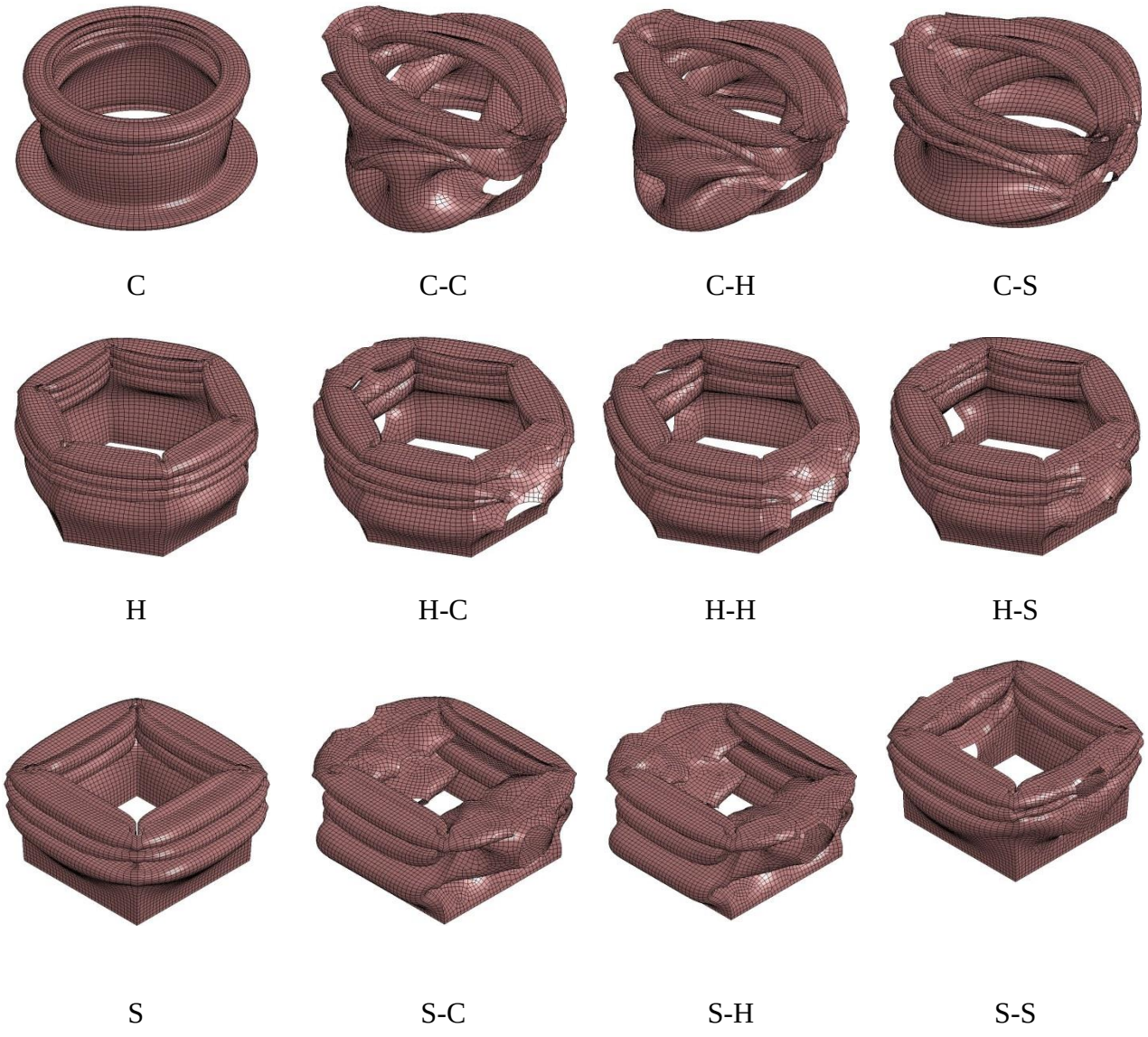

Figure 12: Deformation modes of simple and windowed tubes

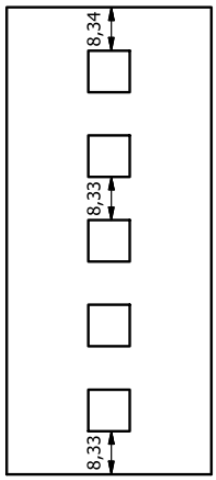

C-S-1

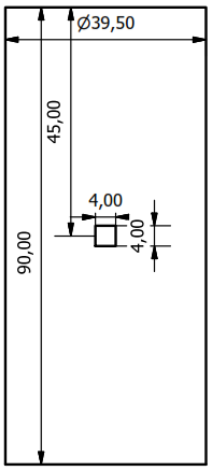

C-S-2

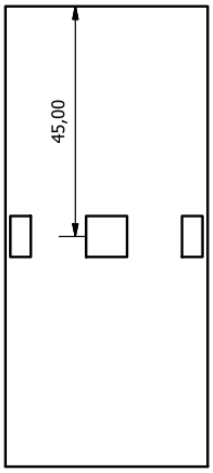

C-S-3

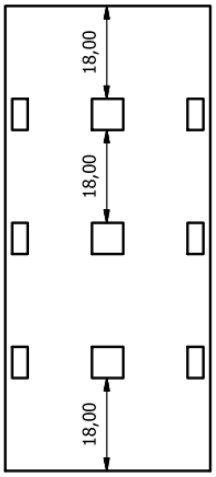

C-S-4

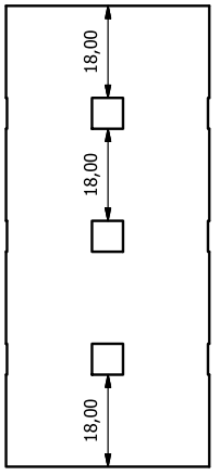

C-S-5

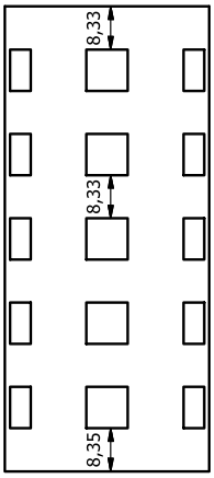

C-S-6

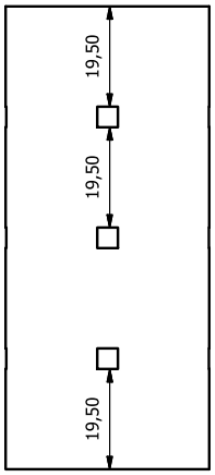

C-S-7

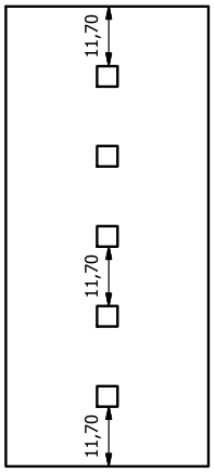

C-S-8

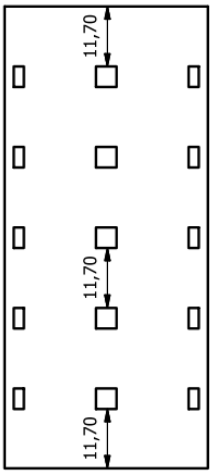

C-S-9

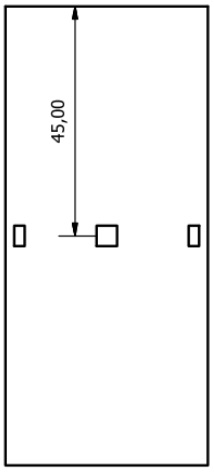

C-S-10

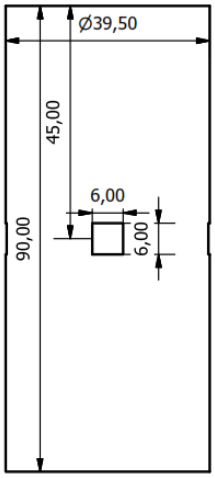

C-S-11

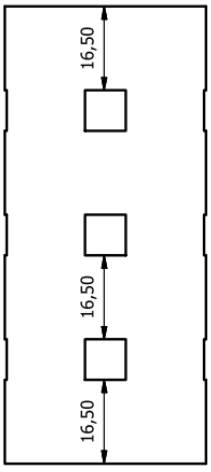

C-S-12

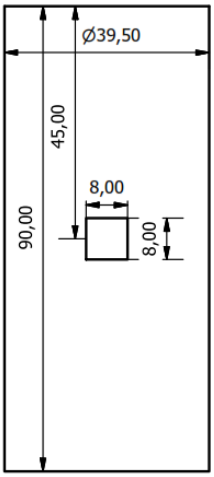

C-S-13

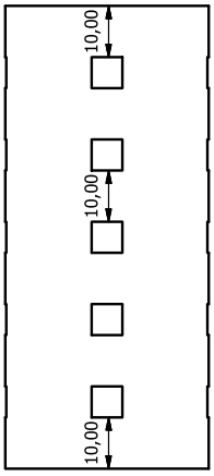

C-S-14

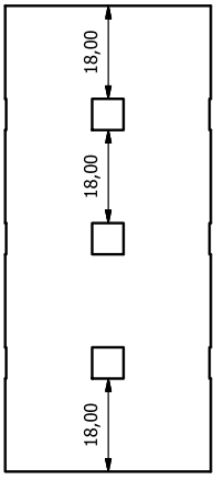

C-S-15

Figure 13: Geometry of C-S windowed tubes used to construct RS models

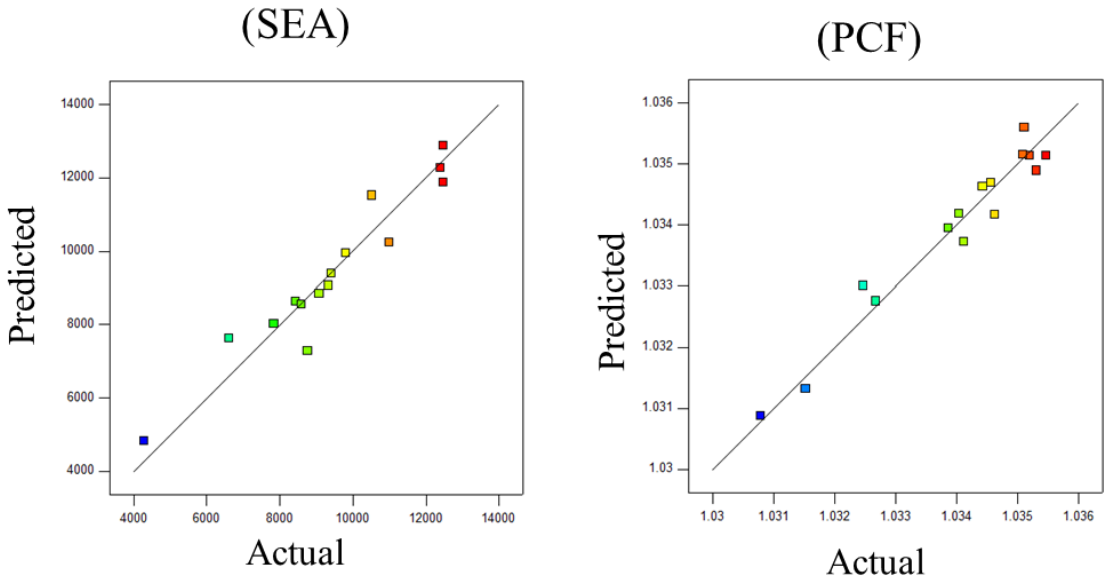

Figure 14: Comparison of FE simulations values against predicted values obtained from RS models at the design points

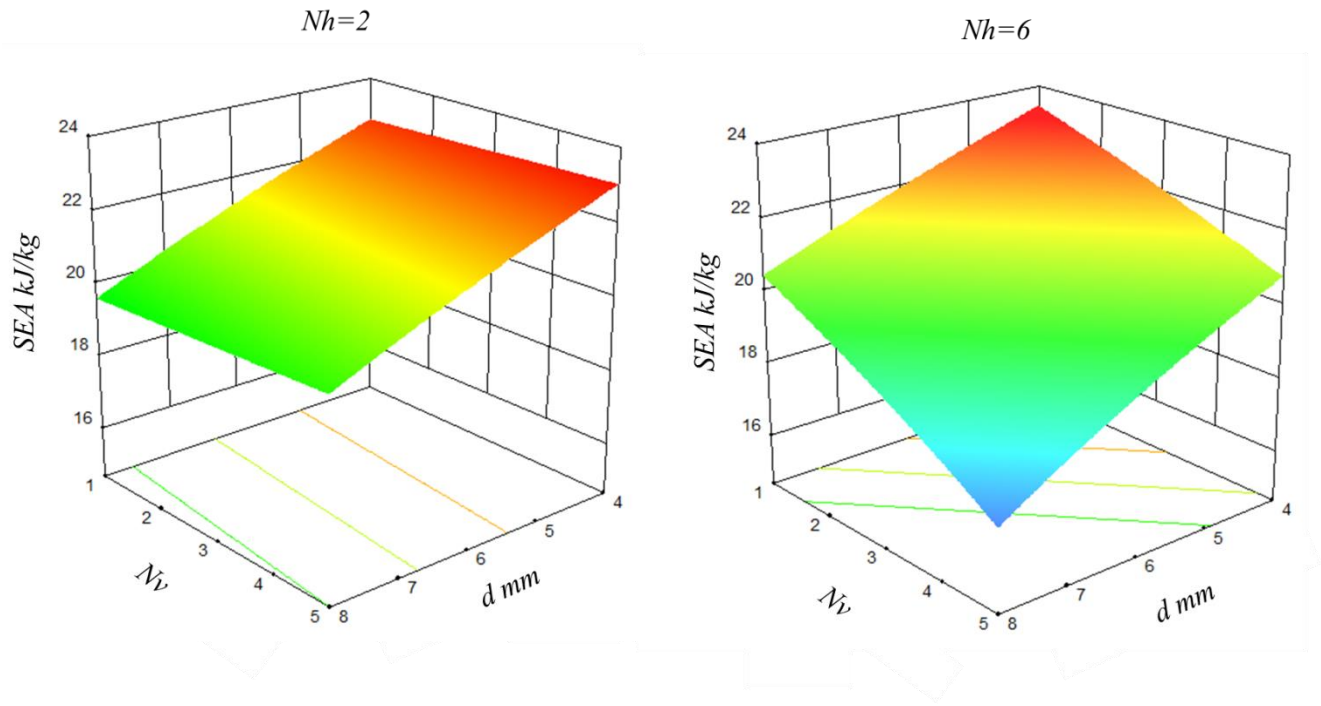

Figure 15: The influence of window parameters on SEA

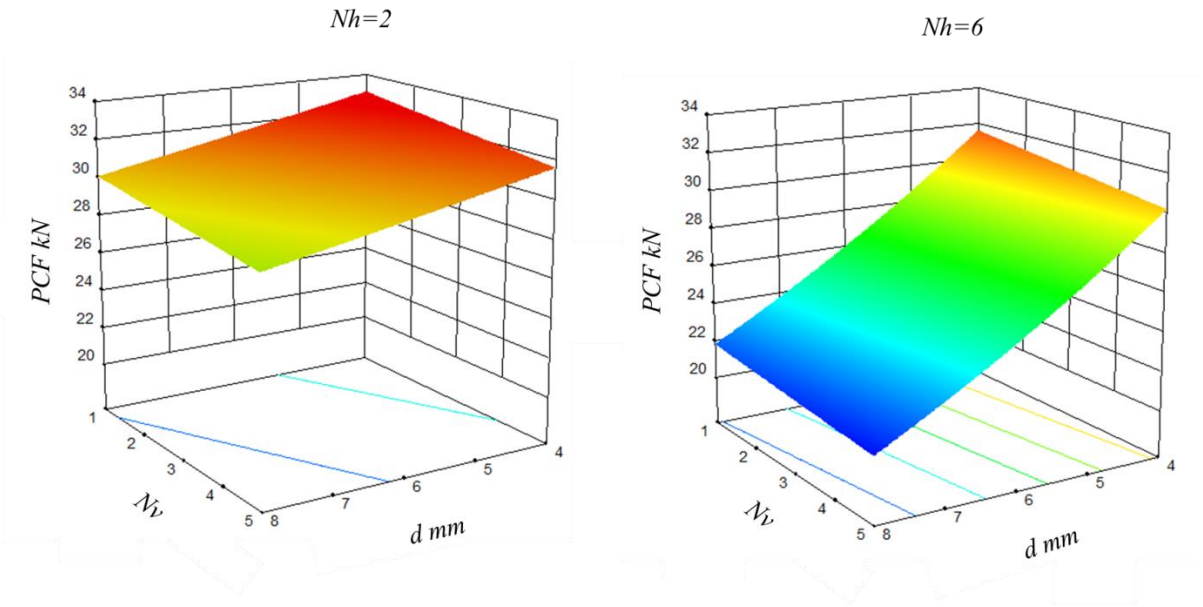

Figure 16: The influence of window parameters on PCF

C-S-1

C-S-2

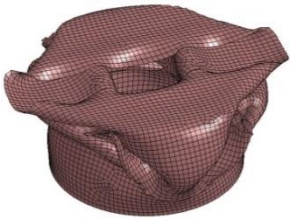

C-S-3

C-S-4

C-S-5

C-S-6

C-S-7

C-S-8

C-S-9

C-S-10

C-S-11

C-S-12

C-S-13

C-S-14

C-S-15

Figure 17: Deformation mode of circular windowed tubes

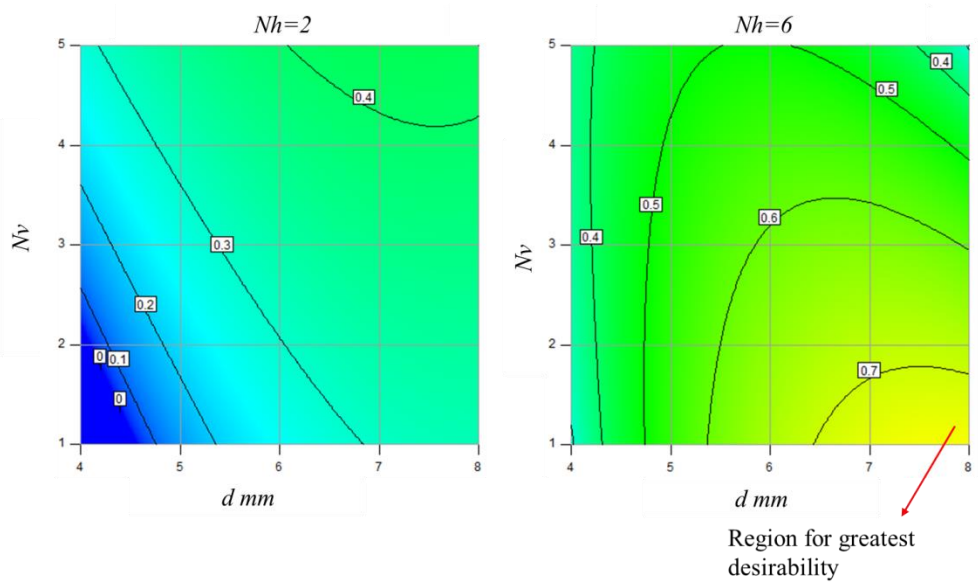

Figure 18: Variation of desirability objective with design variables

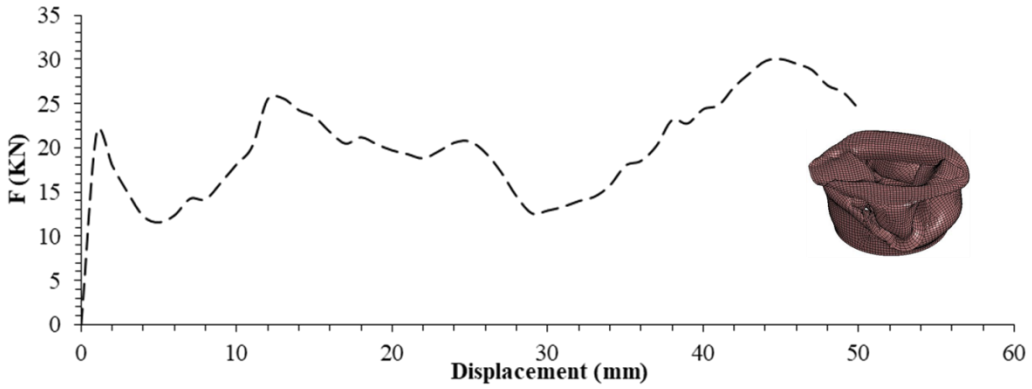

	FE	RS	RE%
SEA (kJ/kg)	21.63144	20.49179	5.268486
PCF (kN)	21.75	21.86948	0.549316

Figure 19: Numerical results of the optimal tube